

Talking to the Airgap: Exploiting Radio-Less Embedded Devices as Radio Receivers

Paul Staat^{1,*}, Daniel Davidovich^{1,*} and Christof Paar^{*}

^{*}Max Planck Institute for Security and Privacy, Bochum, Germany

E-Mail: {paul.staat, daniel.davidovich, christof.paar}@mpi-sp.org

Abstract—Intelligent electronics are deeply embedded in critical infrastructures and must remain reliable, particularly against deliberate attacks. To minimize risks and impede remote compromise, sensitive systems can be physically isolated from external networks, forming an *airgap*. Yet, airgaps can still be infiltrated by capable adversaries gaining code execution. Prior research has shown that attackers can then attempt to wirelessly exfiltrate data across the airgap by exploiting unintended radio emissions. In this work, we demonstrate reversal of this link: malicious code execution on embedded devices can enable wireless *infiltration* of airgapped systems without any hardware modification. In contrast to previous infiltration methods that depend on dedicated sensors (e.g., microphones, LEDs, or temperature sensors) or require strict line-of-sight, we show that unmodified, sensor-less embedded devices can inadvertently act as radio receivers. This phenomenon stems from parasitic radio frequency (RF) sensitivity in PCB traces and on-chip analog-to-digital converters (ADCs), allowing external transmissions to be received and decoded entirely in software.

Across twelve commercially available embedded devices and two custom prototypes, we observe repeatable reception in the 300–1000 MHz range, with detectable signal power as low as 1 mW. To this end, we propose a systematic methodology to identify device configurations that foster such radio sensitivities and comprehensively evaluate their feasibility for wireless data reception. Exploiting these sensitivities, we demonstrate successful data reception over tens of meters, even in non-line-of-sight conditions and show that the reception sensitivities accommodate data rates of up to 100 kbps. Our findings reveal a previously unexplored command-and-control vector for air-gapped systems while challenging assumptions about their inherent isolation. Thereby we highlight the need to reconsider emission and reception security and reveal new security risks in embedded platforms.

1. Introduction

Intelligent electronics are ubiquitous, found in everything from personal devices to safety-critical applications in automotive, aerospace, medical, and industrial domains. In such environments, system reliability is essential, as failures may cause severe economic losses or compromise critical infrastructure. To minimize risks from malicious or

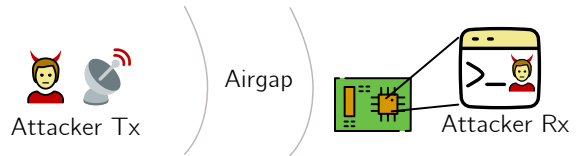


Figure 1: Attack scenario considered in this work. The attacker can execute code on an air-gapped embedded device and attempts receiving modulated radio signals.

accidental external influence, safety and security designers often rely on *airgaps* – rigorous physical isolation of sensitive systems and networks from external connectivity [21], where persistent communication with the outside world is avoided and data transfer is strictly controlled.

While airgaps impose a significant barrier, they do not guarantee immunity to remote attacks. That is, motivated and potent adversaries can still succeed to attack air-gapped environments. A notable example is the 2010 *Stuxnet* attack against industrial control systems in Iran, causing damage of Uranium enrichment centrifuges [39]. Initial infiltration can be accomplished through, e.g., hardware Trojans [50], supply chain compromises [55], or portable USB flash drives [39]. Once attackers can execute malicious code on the air-gapped system, they can attempt *bridging* the airgap by establishing persistent and unconstrained wireless communication with the outside world to reduce communication latency and minimize risk of detection. Given the absence of wireless communication capabilities, however, the attacker must rely on the available hardware resources to unconventionally realize wireless data transfer.

The challenge of *exfiltrating* information from air-gapped systems is well-understood and has been addressed by a large body of research over the past 25 years, including [4], [24], [36], [37], [43], [64]. In particular, all kinds of leakage sources were studied, e.g., electromagnetic, magnetic, vibration, acoustic, optical, thermal, including techniques to accommodate arbitrary complex modulation schemes [4].

In contrast, in this work, we focus on the opposite direction – *infiltrating* information into an air-gapped device on which an attacker can execute code, cf. Figure 1. This enables command-and-control capabilities, allowing the attacker to issue dynamic instructions and adapt their behavior. Such techniques have only received relatively little attention and to the best of our knowledge there are only

¹ These authors contributed equally to this work.

five previous works, as summarized in Table 1. However, the known methods face limitations which significantly limit their threat potential. First, they require the availability of dedicated sensing hardware such as temperature sensors, LEDs, microphones, or cameras. Second, the transmitter and the air-gapped target receiver need to be in close proximity or in line of sight, significantly constraining the attacker’s transmit location. Third, most methods are limited to very low communication rates.

TABLE 1: Communication Into Airgap Systems

Method	Dedicated sensor	Max. dist.	NLOS	Bitrate in bps
Temperature [24]	Temperature	0.4 m	no	0.002
Laser [37]	LED	25 m	no	18,200
Ultrasound [26]	Microphone	8 m	no	166
Infrared [20]	Camera	130 m	no	100
Radio [33]	Temperature	20 m	(yes)	2.5
Radio (this work)	none	20 m	yes	1,000 (up to 100,000)

We overcome the limitations of prior airgap infiltration techniques, presenting a novel approach for wireless infiltration of air-gapped systems that requires no hardware modification and no sensors: We show that unintended electromagnetic sensitivity of commodity embedded devices can be exploited to receive malicious communication signals using only software running on the target device. Intentional electromagnetic interference (IEMI) has been studied as a threat to sensor integrity [31], [42], [61], and Kasmi et al. [33] explored the idea of using IEMI as a communication channel. However, their approach requires a temperature sensor and extreme transmission power of 3.100 W to bridge 20 m at 2.5 bps. In contrast, we achieve 1 kbps over the same distance with just 20 W. Our technique works even in non-line-of-sight scenarios, including through concrete walls, and operates entirely on standard microcontroller units (MCUs) without hardware changes.

In our adversary model, the attacker has code execution on the target device, for example via a malicious firmware update. Once the code runs, it repurposes existing peripherals and on-chip components to implement a lightweight radio receiver capable of demodulating external signals. To this end, we solved three core challenges:

- C1: Absence of wireless components.** Without dedicated wireless hardware, fundamental receiver building blocks – such as the antenna, amplifiers, and frequency conversion – must be substituted.
- C2: Finding reception sensitivities.** Identifying software-controlled peripheral settings and operating modes that produce measurable RF sensitivity requires a systematic discovery methodology.
- C3: Constrained computational resources.** The attacker must receive digital information on tightly constrained low-resource devices while coping with signal impairments.

Our solution for C1 is based on the observation that standard printed circuit board (PCB) traces can unintentionally

act as antennas in the ultra-high frequency (UHF) range between 300 MHz and 1000 MHz. When interfacing with GPIO pins of, e. g., a MCU, device-intrinsic non-linearities yield frequency down-conversion to baseband [31], [38], [67], translating RF energy into DC signals. By employing on-chip ADCs, the attacker can subsequently capture the signals and demodulate them in software.

To address C2, we propose a method for systematic testing of embedded devices for susceptibility to radio-based infiltration: While configuring various on-chip peripherals, we observe the device’ response with and without being exposed to a controlled radio signal. This allows us to estimate the signal-to-noise ratio (SNR) and identify device configurations that maximize the likelihood of fostering radio sensitivity. We assess the prevalence of such effects in a total of 14 real-world devices, including commercially available air-gapped hardware wallets for cryptocurrencies, and find that *all* exhibit significant reception capabilities. We comprehensively characterize the identified RF sensitivities, showing stability across time, location, orientation, and different device samples.

For C3, we show that successful reception is possible using lightweight software-defined receiver algorithms well-suited for implementation on embedded platforms. The adaptive processing tackles signal imperfections and can recover transmitted digital data error-free even without error correction techniques. While we demonstrate a practical wireless link at 1 kbps, we also show that data rates of up to 100 kbps are technically feasible.

Taken together, our findings demonstrate the feasibility of radio wave-based air-gap infiltration, showing that command-and-control capabilities pose a realistic threat requiring only close physical proximity to a compromised target. This contrasts with prior work relying on targeted sensor stimulation. Beyond air-gapped settings, the underlying mechanism may also enable communication between otherwise isolated embedded subsystems. At the same time, our work offers a constructive path forward: by systematically uncovering and characterizing RF sensitivities, our methodology enables proactive identification of vulnerabilities and supports the design of embedded systems with improved electromagnetic resilience.

Contributions. To the best of our knowledge, this is the first work to demonstrate radio wave-based infiltration of air-gapped embedded systems without relying on sensors or line-of-sight transmission. Our key contributions are:

- We show that unmodified, sensor-less embedded devices can act as unintended radio receivers and support covert wireless command-and-control.
- We develop an automated methodology to find RF sensitivities and apply it to 14 platforms (12 commercial devices—including hardware wallets and a drone—and two custom PCBs), identifying vulnerable reception paths and configurations.
- We quantify reception behavior across power, frequency, orientation, timing, and device variants, and report bit-error performance and practical link distances.

- We evaluate signal-integrity-aware PCB design and shielding techniques as countermeasures.
- We will release firmware for sensitivity testing on eight STM32 MCUs, design files for our custom PCBs, and the software-based receiver implementation.

Responsible Disclosure. Our experiments demonstrate RF sensitivities in real-world hardware but did not uncover any immediate security vulnerabilities affecting users of the evaluated products. We followed responsible disclosure practices by informing the respective manufacturers, enabling them to independently assess any potential implications.

2. Preliminaries

In this section, we provide technical background on radio receivers and sensitivity of electronic components for electromagnetic signals and define the threat model considered in this work.

2.1. Technical Background

Conventional Radio Reception. Conventional radio receivers consist of several fundamental components. Here, we provide a brief overview of one simplistic architecture, as illustrated in Figure 2a. The receiver uses an *antenna* to capture radio signals from the air and convert them into electrical signals. The received signal is amplified by a *low-noise amplifier* (*LNA*) to improve sensitivity. A *mixer*, driven by a *local oscillator*, shifts the frequency of the received RF signal, enabling frequency translation to an intermediate frequency or baseband. A *band-select filter* removes out-of-band signals before the signal is digitized by an *ADC*. The digitized signal is then processed through *digital signal processing*, allowing software-defined reception [18]. Modern receiver designs can also perform frequency translation and filtering entirely in the digital domain, for example, through direct-RF sampling where the output of the LNA is digitized directly.

Electromagnetic Sensitivity of Electronics. The electronic circuits of computer systems are inherently vulnerable to electromagnetic interference (EMI) due to their physical nature. EMI can originate from both natural and man-made sources, degrading the performance and reliability of an electronic system [14], [17]. Interference can couple into a device through conductive, inductive, capacitive, or radiative mechanisms [34]. Wires such as PCB traces can act as antennas, allowing electromagnetic energy to reach digital or analog components [2]. Although peripheral sampling rates are often much lower than the signal frequency of EMI, nonlinearities in amplifiers, ADCs, and other components can mix, rectify, or demodulate high-frequency disturbances, producing low-frequency variations or DC offsets that can propagate through and affect the system [31], [54]. On digital data lines, this may produce bit flips [10], [69]; on analog signal lines, sensor readings or ADC outputs can be distorted [48], [54].

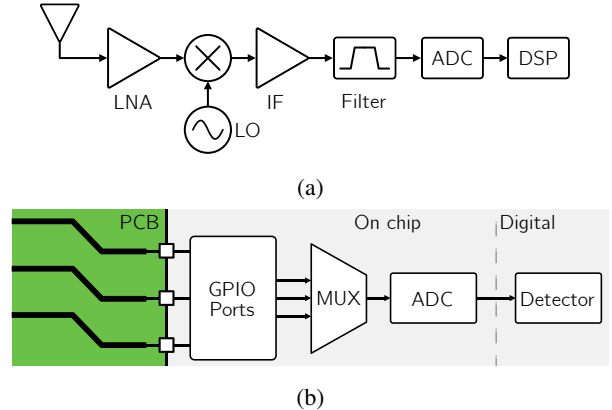


Figure 2: (a) Classical frequency-tuned RF receiver. (b) Embedded device-based radio receiver.

This topic is a major concern for safety-critical domains, including medical, aviation, and automotive applications [34], [65]. Thus, there are extensive efforts in electromagnetic compatibility (EMC) research [51], [52] and regulations [6], [15], [28] to mitigate the risk of EMI.

2.2. Threat Model

Attacker Capabilities. The adversary has software-only access to an air-gapped embedded device such as a MCU or field-programmable gate array (FPGA) and obtained low-level code execution privileges. This includes full control over software and peripheral configuration, as well as access to on-chip ADC readings. However, the adversary cannot alter the device's hardware, add external components, or modify the physical environment of the target. In addition, the adversary can position an external radio transmitter in range of the target and can adjust its transmission parameters, including power, frequency, and modulation.

Goals. The adversary seeks to establish a covert wireless communication channel into the air-gapped system. Specifically, the objective is to transmit arbitrary digital data from the external transmitter to the compromised device using only existing hardware capabilities.

Assumptions. The attacker may select any transmitter position which allows sufficient RF signal power to reach the target device, implying that the physical environment allows signal propagation to the target device, including non line-of-sight (NLOS) scenarios. The attacker can transmit arbitrary waveforms and does not have to comply with regulatory constraints on signal strength or spectrum use.

The target device intended for radio reception remains unmodified and has no radio capabilities by design. Since the attacker has no physical access to the device, they cannot make hardware alterations. However, we assume the attacker is aware of the hardware design of the target device, e.g., being in possession of design files for custom hardware or identical commodity hardware.

3. Our Approach: Embedded Devices as Radio Receivers

In this work, we investigate how radio-less embedded devices can be exploited as unintended wireless receivers—enabling, for example, covert communication into air-gapped environments. Our approach builds on the hypothesis that embedded systems may exhibit measurable responses when exposed to RF signals. A key challenge, however, lies in identifying such RF sensitivities—if they exist—and determining whether they can support the reception of structured communication waveforms. To address this, we present a systematic framework and experimental setup to detect RF sensitivities in real-world devices, forming the foundation for their subsequent characterization (Section 5) and practical exploitation for wireless communication (Section 6).

3.1. Our Idea

Motivated by the literature on EMI [17], [34], [45] and IEMI [48], [57], [61], we hypothesize that commodity embedded devices—composed of many passive and active electronic elements—can behave as crude radio receivers. Unlike EMI and IEMI, which emphasize disruptive or destructive effects of electromagnetic interference, our interest is in detectable RF sensitivities that do not cause device malfunction but nevertheless inject incident RF energy into observable digital traces.

Direct electromagnetic fault injection into digital logic is well known [8], [11], but typically requires very strong fields, risks damaging the target, and is impractical for reliable, long-range information transfer. By contrast, nearly every modern MCU includes on-chip ADCs that can be connected to a variety of internal and external connections. We therefore use these readily available ADCs as the analog–digital bridge for sensing incident RF energy. However, an ADC alone does not make an RF receiver: whether and how an on-chip ADC responds to an RF stimulus depends on coupling mechanisms in the board and chip. To discover useful sensitivities we perform an exhaustive search across the following three key dimensions.

Reception Paths. For a given device under test (DUT), the available reception paths are defined as the set of all possible connections that any internal ADC can be connected to. This may include general-purpose input/output (GPIO) pins, internal sensors such as temperature and voltage monitors, connections to other peripherals such as operational amplifiers, and reserved (undocumented) configurations of the ADC configuration registers. The available reception paths of a DUT are determined by the number of ADCs and the number of MUX connections, see Figure 2b.

Path Configurations. For any reception path that eventually connects to a physical pin of the MCU, the GPIO front end provides additional configuration options that may affect the electrical characteristics, such as pin direction, pull-ups/pull-downs, and input impedance.

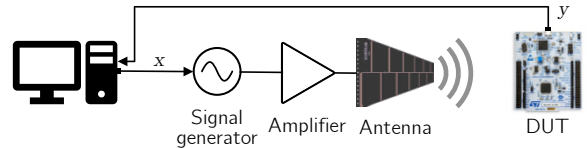


Figure 3: Illustration of our experimental setup.

Transmit Signal. Given that an RF sensitivity on a particular combination of a reception path and configuration exists, the incident RF waveform must match in terms of carrier frequency and signal power. We can denote the stimulus signal $x(t)$ as follows:

$$x(t) = \sqrt{P_{Tx}} m(t) \cos(2\pi f_{Tx} t) \quad (1)$$

where P_{Tx} is the transmit power, $m(t)$ is an amplitude-modulation, and f_{Tx} denotes the carrier frequency.

3.2. Experimental Setup

To systematically search for RF sensitivities, we built a controlled measurement setup as illustrated in Figure 3. A central control computer orchestrates the experiment, configuring both the transmitter and the DUT receiver, triggering measurements, and collecting all captured samples for analysis. All experiments are conducted inside a shielded environment to avoid interference with other radios.

As a programmable RF signal source, we employ a SignalHound VSG60 vector signal generator to precisely control the signal power P_{Tx} from -40 dBm to -7 dBm and vary the signal frequency f_{Tx} between 200 MHz and 1000 MHz. The generator output is amplified by a Mini-Circuits ZHL-20W-13SW+ power amplifier providing approximately 50 dB of gain and enabling transmit powers up to 43 dBm (≈ 20 W). The signal is emitted by an RF-space LPDA-max antenna that has a gain of approximately 6.5 dBi. Unless stated otherwise, the antenna is placed at a distance of 1 m from the DUT.

The DUT represents an embedded system that, in principle, can be any device equipped with an ADC, a serial communication interface, and that we can program the firmware on. Unless otherwise noted, we employ an unmodified Nucleo G474RE development board featuring an STM32 MCU as the main exploration platform. Beyond this reference platform, we further evaluate 13 other devices such as commercially available cryptocurrency hardware wallets based on seven other MCUs (see Section 4). The available reception paths vary by device, e. g., depending on the number of GPIO pins, internal ADC channels, and select on-chip signals. For the path configurations, we consider 64 combinations of the GPIO parameters mode (input, output, analog, alternate function), pud (pull-up / pull-down / none / reserved), value (high, low), output type (open-drain / push-pull). We also configure the ADC parameters, including the total number of samples per reading, the sample rate, and oversampling.

The host computer communicates with the DUT through a serial interface to configure the MCU to a specific combination of reception path and path configuration, trigger an ADC sampling operation, and retrieve the resulting samples for offline processing. This automated workflow enables exhaustive exploration across reception paths, pin configurations, and transmit signal parameters, forming the foundation for our systematic identification of RF sensitivities and their subsequent exploitation.

3.3. Finding RF Sensitivities

We take a phenomenological, measurement-driven approach, empirically characterizing how embedded devices respond to controlled RF stimuli (unmodulated carrier signals at full transmit power). Our RF sensitivity search proceeds exhaustively: We first select a specific reception path-configuration pair on the DUT. We then collect a block of N ADC samples with the RF generator turned off, followed by another block with the generator turned on. This process is repeated while stepping the carrier frequency, producing a frequency sweep for each possible combination of reception path configuration pair.

Using this method, we characterize all 87 reception paths of the Nucleo-G474RE development board, each tested under 64 distinct path configurations and 81 evenly spaced carrier frequencies between 200 MHz and 1000 MHz. For each combination, we collect 32 ADC samples for both the RF-on and RF-off states. To determine whether a given configuration exhibits sensitivity, we apply the analysis pipeline illustrated in Figure 4. Specifically, we compute the mean of each ADC sample block and evaluate the mean difference between the RF-on and RF-off states across frequency steps. This differential trace captures the device’s response to incident RF energy. Finally, we estimate the corresponding SNR using the noise variance observed in the RF-off measurements. The frequency-dependent SNR estimates of three representative and particularly sensitive path-configuration combinations are shown in Figure 5.

We plot the resulting peak SNR across frequencies for each path-configuration combination on the Nucleo-G474RE board and the Passport hardware wallet in Figure 6. Both devices exhibit pronounced RF sensitivities, with several configurations achieving SNRs above 20 dB. The Nucleo-G474RE generally shows stronger and more frequent responses, yet in both devices, the reception path and its specific configuration strongly influence the observed SNR. Notably, in the lower sections of both heatmaps, we observe regions of elevated sensitivity corresponding to path configurations where the GPIO is set to analog mode. On the Nucleo-G474RE, additional peaks appear around configuration indices 10, 20, and 35, where pull-down or pull-up resistors are activated, also resulting in higher SNR.

Manual inspection of all 64 configurations reveals significant redundancy: many configurations produce largely similar responses. Our analysis indicates that the primary factors governing RF sensitivity are the GPIO input mode and the pull-up/pull-down resistor settings. Based on these

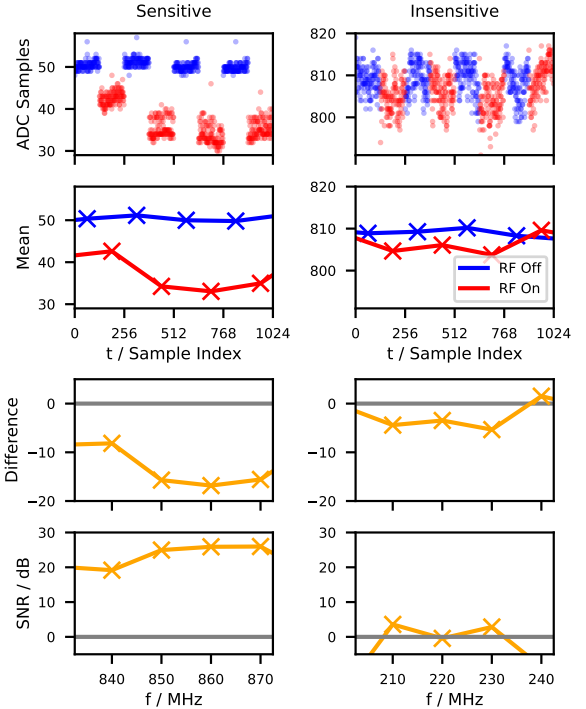


Figure 4: Processing for RF sensitivity testing. First row: raw ADC samples from the device over time while the transmitter is switched on and off and changing frequency. Second row: average over sample blocks. Third row: Difference of block averages between on and off samples over frequency. Fourth row: SNR estimation over frequency.

insights, we distilled a subset of 8 recommended path configurations (see Appendix C), sufficient to characterize most sensitivity patterns. Figure 7 illustrates this for two reception paths on the Nucleo-G474RE: the plot compares sensitivity spectra across all configurations and highlights the recommended subset, demonstrating that these selected configurations effectively capture all distinct classes of RF sensitivity. Apart from the path-configuration combination, we found that the ADC-based sampling configuration affects the SNR. As expected, oversampling can be used to enhance ADC resolution and mitigate noise, thereby improving SNR. SNR results for varying oversampling ratios can be found in Appendix Section A.

4. How Common are RF Sensitivities in the Wild?

So far, we have outlined and demonstrated our methodology for identifying RF sensitivities on two representative devices. On both the Nucleo-G474RE board and the Passport hardware wallet, we found clear sensitivities with SNRs sufficiently high to enable covert wireless communication. A natural next question is whether these are device-specific isolated observations or whether such RF sensitivities are a more widespread phenomenon among embedded devices.

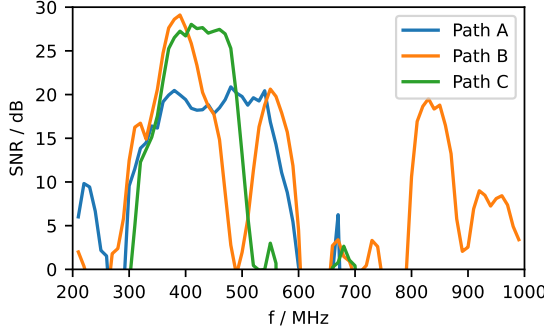


Figure 5: SNR over frequency for three different reception paths on the Nucleo-G474RE board.

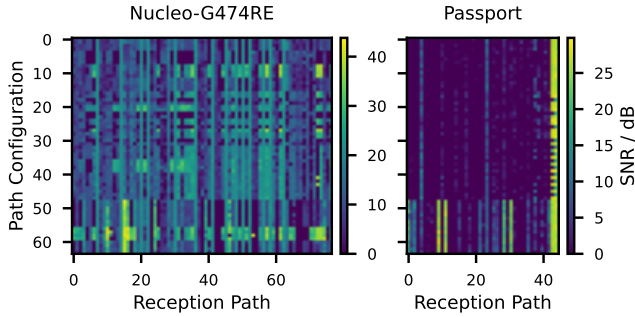


Figure 6: Full sensitivity testing experiment results for the Nucleo-G474RE ⑩ and the Passport ⑤ boards, showing the peak SNR over frequency for combinations of reception path and GPIO configuration.

To investigate this, we ran our sensitivity discovery method on a total of 14 devices, comprising 12 commercial products and 2 custom devices. Our selection includes eight cryptocurrency hardware wallets (some of which are explicitly advertised as air-gapped), an electronics hobbyist drone, multiple MCU development boards, and two custom PCBs (see Section 7 for details on the custom designs). The tested devices are depicted in Figure 8. Based on the insights gained from testing the Nucleo-G474RE and the Passport, we restricted our search across path configurations to the

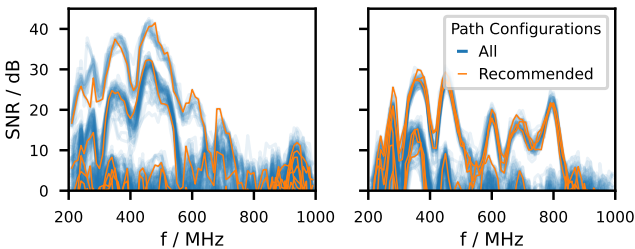


Figure 7: SNR over frequency on two reception paths for all 64 possible path configurations and the recommended path configurations.

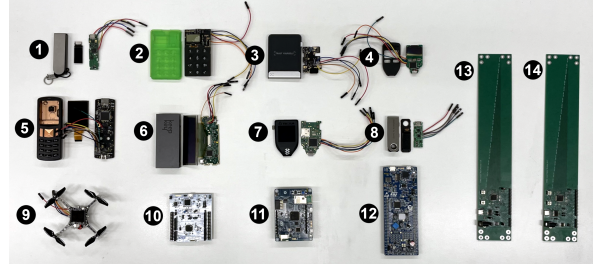


Figure 8: All tested devices.

8 recommended choices, varying the GPIO input mode and pull-up/down configurations.

For the cryptocurrency wallets, we de-soldered the original MCUs and replaced them with identical, blank parts to obtain full firmware control over the hardware platform. Our goal in doing so was strictly to evaluate RF reception characteristics—not to target secure boot or similar protection mechanisms. Attacks to break such mechanisms have been studied extensively in prior work [8], [56], [63] and are orthogonal to our contribution. To ensure comparability, we conducted all experiments on the bare PCBs of the devices, thereby isolating the fundamental receive mechanism from potential effects of device enclosures or shielding. While our preliminary results indicate that reception sensitivities persist when devices are enclosed, we have also observed instances where casing materials partially attenuate the effect. In future work, we will further investigate the influence of enclosures and electronic peripherals.

Table 2 summarizes the results for all tested devices. For each device (cf. the numbering in Figure 8), we list the MCU model, the number of sensitive versus total reception paths, the most sensitive path and its configuration (if applicable), the frequency range of observed sensitivity, and the peak measured SNR. The central finding is clear: *every* tested device exhibited measurable RF sensitivity. This confirms that the phenomenon is not tied to a particular hardware design, but rather a recurring effect that manifests broadly across embedded platforms. In several cases, the incident RF signal induced large shifts in ADC traces that otherwise show no variance; for such cases, the SNRs could not be reliably estimated and are therefore reported as “high”. At the same time, the results reveal pronounced variation across devices: while some, such as the Ledger Nano S Plus and Ledger Flex, exhibit only weak sensitivity, others, such as the COLDCARD™ Mk4, the Passport, and our custom PCB, show stronger and more sensitivities.

5. Sensitivity Characterization

In this section, we systematically characterize the RF sensitivities of the Nucleo-G474RE board, analyzing their stability over time, device dependence, and sensitivity to orientation.

TABLE 2: Sensitivity results for all tested devices.

Device	Microcontroller	Sensitive Paths	Best Reception Path	Path Configuration	Frequency [MHz]	Peak SNR [dB]
① Ledger Nano X	STM32WB35CC	18 / 44	ADC Channel VREFINT (single-ended)	-	300 - 400, 450 - 650, 735	24
② COLDCARD™ Mk4	STM32L4S5VI	5 / 34	ADC Channel 11, differential-ended with GPIOs PA6 and PA7	analog, pull-down, set	320 - 400, 420 - 530, 660 - 680	high
③ Ledger Flex	STM32WB35CC	2 / 44	ADC Channel VREFINT (single-ended)	-	500 - 600	12
④ Trezor Model One	STM32F205RE	5 / 43	ADC2 Channel 7 with GPIO PA7	analog, pull-up, reset	250 - 525	15
⑤ Passport	STM32H753VI	24 / 45	ADC3 Channel VBAT (single-ended)	-	200 - 250, 280, 320 - 1000	34
⑥ KeepKey	STM32F205RG	5 / 43	ADC1 Channel VREFINT	-	350 - 400, 600 - 1000	16
⑦ Trezor Model T	STM32F427VI	13 / 57	ADC3 Channel 17 (reserved)	-	300 - 600	14
⑧ Ledger Nano S Plus	STM32F042K6	5 / 13	ADC Channel 4 with GPIO PA4	input, pull-down, set	325 - 375, 600	11
⑨ CrazyFlie 2.1+	STM32F405RG	19 / 57	ADC3 Channel 11 with GPIO PC1	analog, pull-up, reset	200 - 1000	62
⑩ Nucleo-G474RE	STM32G474RE	53 / 87	ADC2 connected to OPAMP5 with GPIO PC3	AF, pull-down, set	200 - 1000	33
⑪ STM32L4+ Discovery IoT Kit	STM32L4S5VI	9 / 44	ADC Channel 12 with GPIO PA7	input, pull-up, reset	400 - 725, 820 - 850	19
⑫ STM32G474RE Discovery Kit	STM32G474RE	45 / 87	ADC1 Channel 8 with GPIO PC2	analog, pull-down, set	250 - 1000	37
⑬ Custom PCB	STM32G474RE	87 / 87	ADC2 Channel 6 with GPIO PC0	analog, pull-up, reset	200 - 1000	high
⑭ Custom PCB /w ground plane	STM32G474RE	53 / 87	ADC2 connected to OPAMP2 with GPIO PB0	input, pull-up, reset	200 - 1000	high

5.1. Dependence on Signal Power

A critical question is whether the observed RF sensitivities could enable wireless communication over larger distances. To examine this, we repeated the SNR estimation for the sensitivities shown in Figure 5 at fixed frequencies while progressively reducing the transmit power. Using the known antenna–device distance, frequency, and transmission power, we estimated the signal power incident at the DUT. Figure 9 plots the resulting SNR as a function of the estimated receive power, showing that signal powers as low as 0 dBm remain detectable. Interestingly, the SNR increases superlinearly with signal power, indicating the presence of nonlinear effects—a plausible outcome given the unconventional reception mechanism. These results demonstrate that the observed sensitivities persist at lower signal powers rather than disappearing abruptly. In fact, as we will see in data transmission experiments in Section 6, reception on path B extends to even weaker signal levels.

5.2. Stability Over Time

To evaluate the temporal stability of the identified RF sensitivities, we repeat the sensitivity characterization periodically over a 24 h period. In each iteration, we measure the device’s response while alternately enabling and disabling the RF transmit signal. As shown in Figure 10 for two representative reception paths, the frequency-dependent sensitivity patterns remain largely consistent over time. The first path (top) exhibits high stability with nearly unchanged sensitive frequency regions, whereas the second path (bottom) shows moderate drift and both short- and long-term fluctuations, evident from the SNR degradation after approximately 15 h. Overall, these results indicate that the

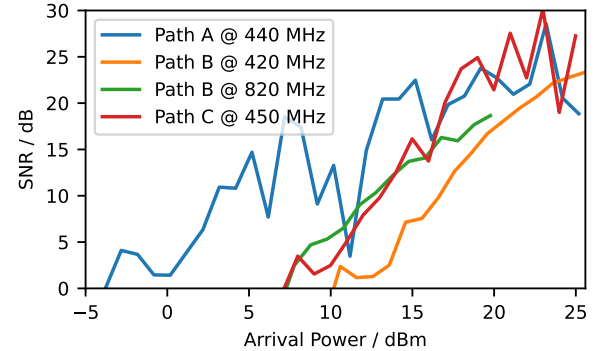


Figure 9: SNR over estimated arrival signal power for three reception paths.

device’s unintended RF reception behavior is persistent and only mildly affected by temporal variations.

5.3. Inter-Device Variation

So far, we have established that RF sensitivities on a given device can exist across several peripheral configurations and remain stable over time. In a realistic airgap infiltration scenario, however, the attacker may not have direct access to the target hardware for characterization. While such access might still be possible—through brief onsite presence or a supply-chain compromise—it is considerably more practical for the attacker to obtain an identical device model and characterize its reception sensitivities in advance [67]. The key question, therefore, is whether RF sensitivities discovered on one sample of a device type are transferable to other samples of the same type.

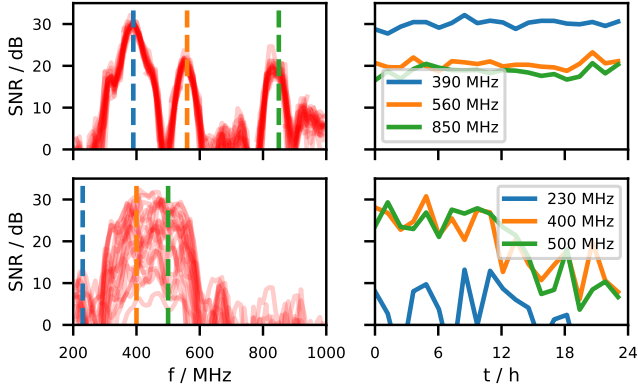


Figure 10: Sensitivity assessment over time for two separate reception paths (top: path B, bottom: path A) over frequency (left) and time (right).

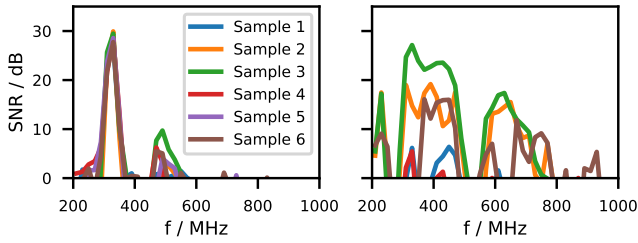


Figure 11: SNR over frequency for two distinct reception paths on six different Nucleo-G474RE boards, showing that sensitivities are repeatable.

To answer this, we examine six Nucleo-G474RE boards under identical test conditions, ensuring consistent placement, orientation, and environmental conditions. Figure 11 shows the measured SNR over frequency for two representative reception paths across all six samples. On the left, we observe near-perfect agreement between devices: the sensitive frequency regions and SNR results align closely across all samples. On the right, however, only a subset of devices exhibit notable sensitivity, while others (e.g., sample 5) show none. Among the sensitive samples, the spectral shape and frequency range of the sensitivities remain largely consistent. In our sensitivity assessments, testing all reception paths with our 8 recommended configuration, we found 55 combinations with RF sensitivity on all six samples. In short, sensitivities are repeatable across device instances: an attacker can reliably identify device-repeatable sensitivities on surrogate units and then transfer those findings to the target device.

5.4. Device Orientation

To assess whether device orientation influences RF sensitivity, we measured the SNR over frequency for two reception paths while systematically changing the device orientation. Specifically, we measured the SNR at a fixed frequency while rotating the device in the *xz* plane. Figure 12

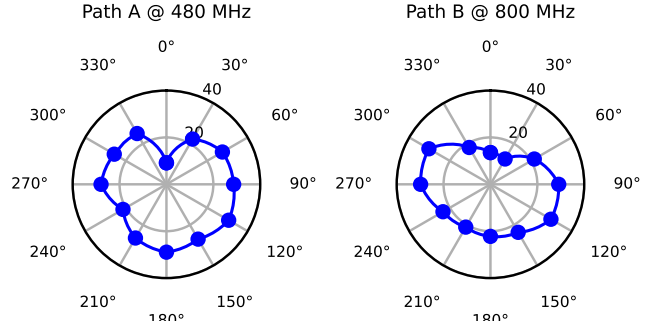


Figure 12: SNRs at a single frequency for two reception paths over device rotation (in the *xz* plane).

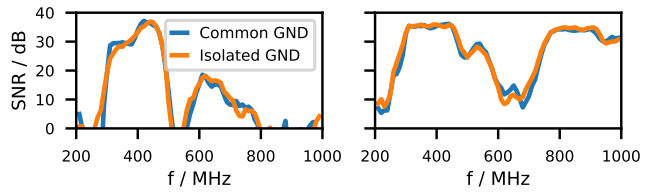


Figure 13: With and without common ground between transmitter and receiver.

shows the results over the DUT angle with respect to the transmitter. Here, we observe slight directionality: Path A shows reduced sensitivity near 0° but remains otherwise stable, whereas path B exhibits stronger responses around 90° and 270° . Further, we found that placing the device in other planes affects the reception sensitivity but does not eliminate the phenomenon as can be seen from the frequency responses shown in Figure 22 in Appendix B.

5.5. Impact of Wired Connections

Next, we examine the influence of wired connections to the DUT, confirming that the observed RF sensitivities stem from the device itself, receiving ambient radio waves.

Common Ground Connection. Figure 13 illustrates the SNR of two reception paths across frequency with and without a common ground connection between the RF transmitter and the DUT. In the common-ground configuration, both devices share the same computer for control and power, as shown in Figure 3. In the isolated-ground configuration, the DUT is powered by a separate, battery-powered laptop, ensuring galvanic isolation. All other experimental conditions remain identical.

As shown in the figure, the sensitivity profiles remain virtually unchanged across both configurations, with nearly identical SNR characteristics for both reception paths. We therefore conclude that the observed reception sensitivities do not result from unintended conductive coupling between the transmitter and the target device, but rather stem from genuine electromagnetic interactions.

USB Connection. Next, we investigate whether the observed RF sensitivities on the Nucleo-G474RE board origi-

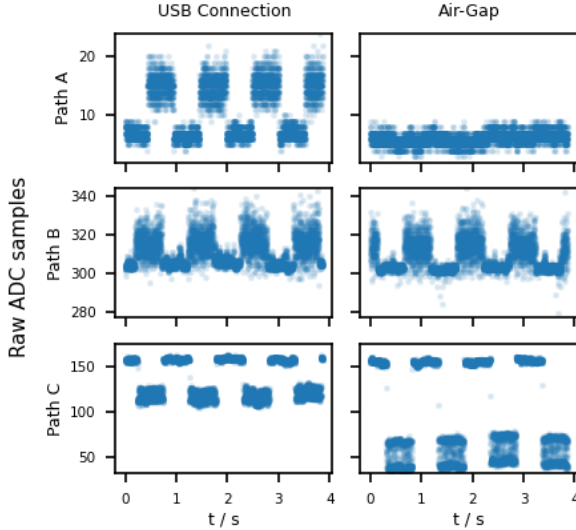


Figure 14: Raw ADC recordings with USB connection (left) and fully air-gapped operation (right) while turning the RF transmission on and off every 0.5 m.

inate from the board itself or from peripheral components—specifically, the USB cable we use for control and data transfer. While external cables can legitimately act as antennas, distinguishing their influence is essential for understanding the reception mechanism and validating the generality of our measurements.

We conduct an experiment where we toggle the RF transmitter on and off 0.5 s while recording ADC samples on the DUT. Crucially, we run this experiment under two conditions: with the Universal Serial Bus (USB) cable connection to the host and in a fully air-gapped configuration, where the DUT is powered by a battery and ADC recording is manually triggered via a physical button press. After each run, the recorded samples are retrieved by reconnecting the serial interface to the experiment computer. This allows us to compare measurements taken with and without the USB cable attached.

Figure 14 shows raw ADC time series for both configurations—USB-connected (left) and air-gapped (right). As evident from the figure, the sensitivity on Path A disappears when the USB cable is removed, suggesting that it was primarily induced by the cable acting as an antenna. In contrast, Path B remains virtually unchanged, while Path C even exhibits stronger sensitivity in the air-gapped case. This confirms that while peripheral components can contribute to reception behavior, observed RF sensitivity can indeed be attributed to intrinsic board-level behavior, independent of external connections.

6. Reception of Communication Signals

We now explore how the identified RF sensitivities can be exploited for wireless data reception. We first characterize bit error rate (BER) and data rate performance, and then

demonstrate a full-blown data reception under real-world conditions over a distance of 20 m.

6.1. Modulation Scheme

Given that the identified RF sensitivities allow reliable distinction between the presence and absence of a carrier, the most natural choice for digital modulation is on-off keying (OOK), where the transmitter is enabled for a 1 and disabled for a 0. In all subsequent experiments, we employ OOK with rectangular pulse shaping. However, since the received signal strength scales with transmit power (see Figure 9), higher-order amplitude-shift keying (ASK), e.g., with four symbols, is in principle feasible.

6.2. Ideal Receiver Bit Error Rates

To assess whether the observed RF sensitivities can be leveraged for wireless data reception, we conducted the following experiment. For a single reception path, we recorded 10,000 ADC sample blocks while the RF signal generator was randomly either switched on or off, effectively emulating an OOK transmission. We assume perfect transmitter-receiver synchronization (i.e., we collect 127 samples per bit) and neglect transient effects between the on and off states. As a simple demodulator, we apply a moving average filter to track slow variations in the direct current (DC) offset, using its output as a decision threshold. Blocks with an average above this threshold are decoded as a ‘1’, and those below as a ‘0’. Comparing the resulting bitstream with the known transmission sequence allows us to compute the corresponding BER.

We repeated this experiment for ten different reception paths and multiple transmit powers. Using the known antenna distance and carrier frequency, we estimate the power arriving at the device (Nucleo G474RE) and plot the resulting BER curves in Figure 15. The results reveal two key findings: (i) reception path B achieves the best performance, with a BER below 2% at an incident power of 0 dBm ($\approx 1\text{ mW}$), and (ii) the achievable sensitivity strongly depends on the chosen reception path. Still, 7 of 10 path reach a BER below 1% when the incident signal power is 10 dBm ($\approx 10\text{ mW}$). The non-monotonic BER curve of path A is due to strong noise and drift on the path. Overall, this experiment demonstrates that the identified RF sensitivities can indeed support reliable digital communication.

Bandwidth Considerations. In the previous experiment, we ignored transient effects introduced by switching the RF carrier on and off. For reliable OOK reception, however, the underlying RF sensitivity must provide sufficient bandwidth so that bit transitions remain distinguishable. To evaluate such effects qualitatively, we configure the Nucleo-G474RE board to reception path B and transmit OOK signals with alternating ‘0’/‘1’ patterns at data rates between 500 bps and 100,000 bps. The ADC sampling rate is adjusted to ensure adequate oversampling for all rates.

Figure 16 shows 20 received bits per rate and we observe that edge steepness reduces with higher data rates, causing

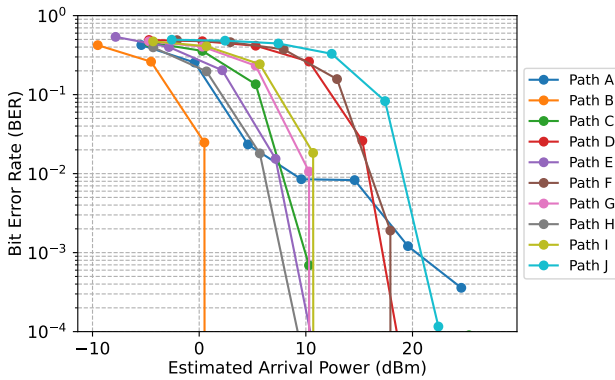


Figure 15: BER for a number of reception paths on the Nucleo-G474RE over estimated received signal power under ideal synchronization.

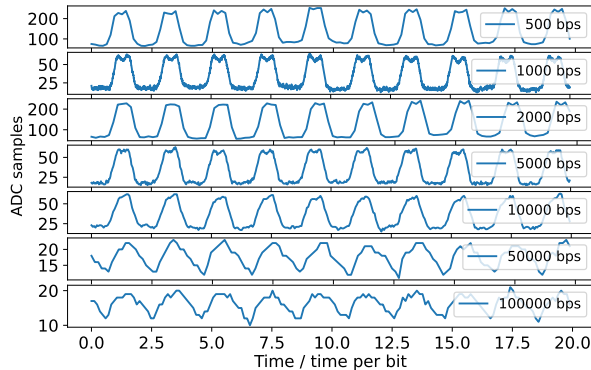


Figure 16: Illustration of receive signal waveform over increasing symbol rates, showing a decreasing slew rate with increasing symbol rate.

increasing smearing between adjacent bits. This result suggests a limited bandwidth of the reception path. Nonetheless, even at 100 kbps, the bit pattern remains discernible.

6.3. Real-World Data Reception

We now demonstrate that an unmodified, radio-less embedded device can reliably receive digital information transmitted over the air—realizing a functional wireless receiver built entirely from unintended RF sensitivities. For this experiment, we configure the Nucleo-G474RE board to use reception path B and place it at distances of 3 m and 20 m from the attacker’s antenna and transmit a random binary sequence of approximately 12,000 bits at a data rate of 1 kbps at 868 MHz and a transmit power of 43 dBm. At the same time, we record the ADC samples from the MCU. The setup is illustrated in Figure 17 (a) and (e). While these photos are provided for clarity, all measurements were conducted in a large, shielded laboratory environment to ensure compliance with emission regulations.

Using standard software-defined radio processing techniques—adaptive scaling, DC offset removal, and symbol-

timing recovery [18], [49]—we decode the received waveforms, as shown in Figure 17 (b) and (f). Correctly decoded bits are marked in green, and errors in red. At 3 m, reception is entirely error-free. Even at 20 m, where the received SNR is substantially lower, the signal remains clearly distinguishable, with only 781 bit errors out of 12,565 transmitted bits ($\text{BER} \approx 6.2\%$). Most residual errors occur in short bursts and could be fully corrected using standard forward error correction codes [18].

Upon closer analysis, we found that the residual bit errors primarily stem from self-interference introduced by the serial data transmission from the MCU to the host computer during sampling. In a practical attack scenario, such interference would not occur, as data would be processed locally on the device. Moreover, we observed that other reception paths did not exhibit this sensitivity during data transfer. A deeper investigation into self-interference caused by device activity and methods to compensate for it remains subject to future work. Initial results indicate that standard processor workloads, such as ongoing computations, do not interfere with the reception.

To assess robustness beyond line-of-sight conditions, we repeated the experiment with the target device placed behind a concrete wall, observing similar signal characteristics and successful frame reconstruction. These findings confirm that unintended RF sensitivities are sufficiently stable and pronounced to support reliable wireless communication over tens of meters without any intentional radio hardware.

7. Countermeasures

In this section, we discuss and evaluate potential countermeasures against wireless communication into air-gapped embedded devices.

Shielding. From a physical perspective, the most straightforward defense against external RF infiltration is electromagnetic shielding. Standards in the TEMPEST domain [7] define stringent limits on electromagnetic emissions and require containment through shielded enclosures. Because electromagnetic shielding is inherently reciprocal, any barrier that prevents emissions from escaping a device should also block external signals from entering it. However, conventional emission security tests focus exclusively on radiation originating *from* the device itself and thus provide no guarantee against signals *entering* the device.

To experimentally assess the effectiveness of shielding in mitigating RF sensitivity, we repeated the experiment from Section 5.5 with the Nucleo-G474RE board in an air-gapped configuration. The ADC recorded samples while the RF transmitter was alternately switched on and off. We repeated the measurement across four conditions: unshielded, enclosed in a plastic case, the same case wrapped in aluminum foil, and the device placed inside a dedicated shielding box.

As shown in Figure 18, introducing a metallic enclosure effectively eliminates the observable reception sensitivity. This confirms that shielding can mitigate the phenomenon.

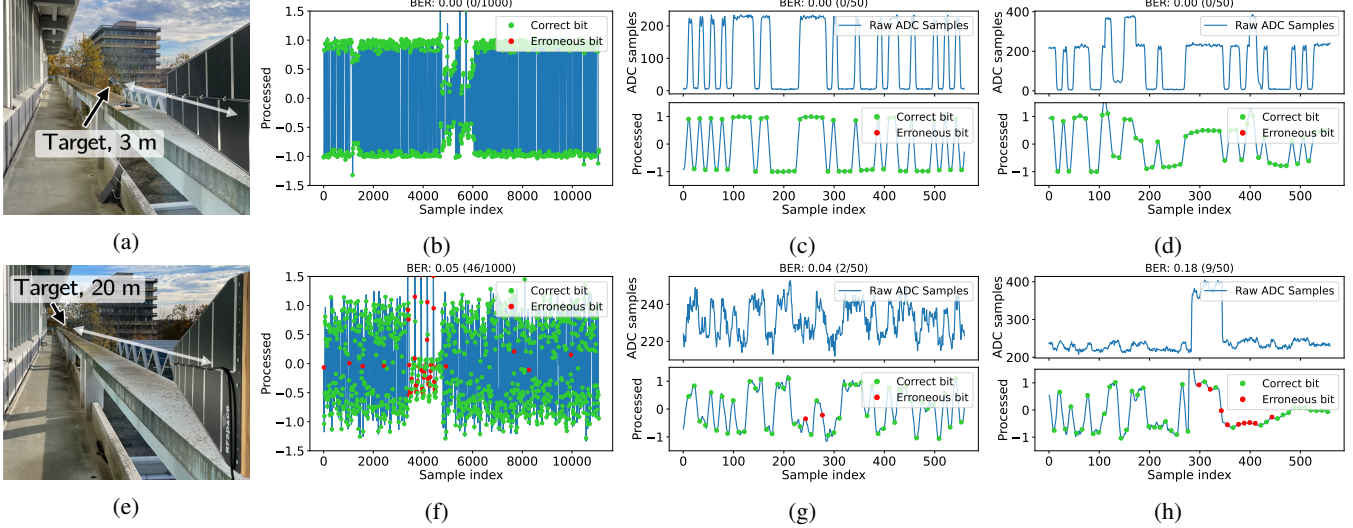


Figure 17: Real-world bit transmission experiment towards the Nucleo-G474RE board at 3 m (top) and 20 m (bottom) distance from the transmitter. (b) and (f): Complete processed receive signals including bit timing. (c) and (g): Raw ADC samples and processed signals including bit timing under ideal conditions. (d) and (h): Raw ADC samples and processed signals during a self-interference event due to serial communication with the host computer.

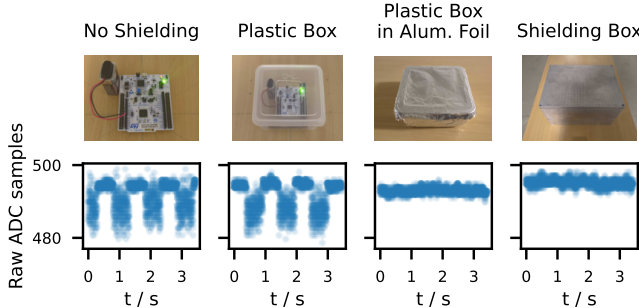


Figure 18: Evaluation of shielding measures.

While this is one particular example, we emphasize that implementing robust electromagnetic shielding in practice is challenging, demanding systematic testing across reception paths to verify the absence of sensitivities.

PCB Design for Signal Integrity. To assess how PCB design practices can mitigate RF sensitivity [46], we fabricated a custom two-layer FR4 PCB with an STM32G474RE MCU, on-board power regulation, a USB interface, and several PCB traces of varying lengths. We produced two otherwise identical boards: one with a continuous ground plane on the bottom layer and one without, isolating the effect of the ground plane on RF sensitivity.

We evaluated both boards under identical conditions, systematically sweeping all reception paths and eight preferred GPIO configurations. The resulting peak SNRs are shown in Figure 19. Both boards exhibit similar structural patterns, highlighting the configurations most prone to external RF energy, yet the ground-plane board shows a consistent overall reduction in sensitivity. As summarized

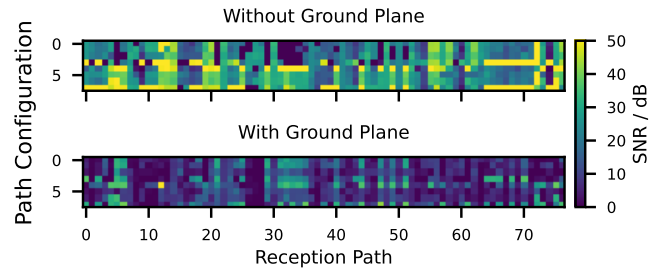


Figure 19: Custom PCB sensitivity testing peak SNR results for all available reception paths and corresponding GPIO configurations.

in Table 2, the board without a ground plane exhibited sensitivity on *all* of the 87 reception paths, whereas the board with a ground plane reduced this to 53 sensitive paths.

Figure 20 further compares the SNR across frequency for two representative paths with and without the ground plane. While spectral shapes remain similar, the ground-plane board achieves more than 20 dB lower sensitivity across the measured frequency range. These results confirm that well-grounded PCB designs with continuous return paths can substantially mitigate unintentional RF coupling. Nonetheless, residual sensitivities persist under specific configurations, underscoring that grounding alone is not a complete solution, demanding additional measures.

Other Countermeasures. Additional defenses include monitoring the RF spectrum for anomalous signals, allowing the defender to detect the attack. Another approach is constant jamming of the airgap environment to make it unusable for

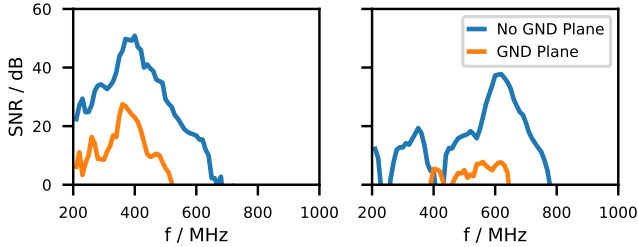


Figure 20: Comparison of reception SNR over frequency on the custom PCB with and without ground plane for two distinct reception paths.

covert communication. Both measures are complementary to shielding and hardware-level protections.

8. Discussion

In the following, we discuss the experimental setup, our results, limitations, and provide directions for future research.

8.1. Experimental Setup and Results

In our experiments, we focused on finding RF sensitivities of embedded devices and exploiting them to receive wireless communication signals. Devices were used as data acquisition platforms, streaming ADC samples over USB to a host computer for offline analysis to facilitate controlled experimentation. In line with our attacker model, which assumes code execution on the target, we deployed custom firmware on all evaluated platforms.

For cryptocurrency hardware wallets, which employ software protections to prevent unauthorized firmware modification, we replaced the original MCU with an identical but unlocked chip. How code execution may be obtained on deployed systems is beyond the scope of this work; in practice, it could arise through established attack classes such as boot process attacks [8], [63] or supply-chain compromise, as previously discussed in the context of cryptocurrency wallets [56].

Our study shows that RF sensitivities are a common characteristic of modern embedded hardware, including security-sensitive platforms, and should not be interpreted as a comparative assessment of product security. Measurements were deliberately conducted on bare PCBs to isolate fundamental physical effects; evaluating fully assembled devices with enclosures and connected peripherals remains for future work. Finally, a real-world air-gap infiltration would require integrating malicious receiver functionality alongside legitimate software, which we believe is feasible with additional engineering effort.

For sensitivity assessment of a DUT, we performed device testing with a priori knowledge of the radio signal, i.e., we recorded labeled observations with the RF signal turned on and off. While this differs from the communication scenario—where the attacker must detect the presence

of a signal without prior knowledge—this setup enables controlled testing for RF sensitivities in a lab environment and serves as a proof of concept for the underlying reception mechanism. As our demonstration of wireless receiver operation shows, the effects are strong enough for blind detection, supporting wireless communication at low error rates.

8.2. Limitations

ADC Availability. A fundamental precondition for exploiting RF sensitivities on radio-less embedded devices is the presence of an ADC that the attacker can access. Without an ADC, the attacker cannot obtain measurable digital values corresponding to analog RF signal variations. Thus, our approach is limited to devices where the attacker can at least observe ADC outputs, while ADC reconfiguration is optional.

Receiver Functionality. As shown, radio-less embedded devices can receive digital communication signals from significant distances, on the order of tens of meters. While some improvement in reception sensitivity may be possible, the potential gains are inherently limited due to the unconventional approach to signal reception. Unlike standard radio receivers, the functionality leveraged here does not provide typical band-selection features. First, the receiver is not frequency-tuned, i.e., there is no local oscillator and thus the receiver cannot distinguish the carrier frequency of received signal. Second, frequency selectivity is determined solely by the frequency response of the specific reception path, which can be relatively broad and may be susceptible to interference. However, given the inherently low sensitivity of the receiver, only particularly strong interference would meaningfully impact reception.

Determining Sensitivity. In this work, we have introduced and demonstrated the fundamental mechanism for receiving radio communication signals on radio-less embedded devices. Our analysis assumes that the attacker possesses enough knowledge about target devices to determine their sensitivities. In scenarios where a reference device is unavailable—such as when targeting custom hardware platforms—the attacker can likely not directly identify optimal transmission frequencies or device configurations. On the receiving side, the attacker may rely on random reception paths, using configurations that have proven effective on similar devices. On the transmitting side, broadband signals can cover multiple potentially sensitive frequencies simultaneously. If real-time feedback from the target device is available, the attacker can further refine both the receiver configuration and transmission parameters through in-situ optimization, adapting based on whether signals are successfully received.

Co-Existence of Functionalities. In our current approach, we reconfigure the peripheral settings of the MCU to connect sensitive traces to an ADC, enabling radio reception. This disables the pin’s native functionality, such as bus communication, during reception. A promising direction

for future work is to preserve pin functionality while still enabling RF reception. This would require a mechanism to simultaneously route the signal to both the peripheral device, e.g., Inter-Integrated Circuit (I2C) or serial peripheral interface (SPI), and the ADC. An attacker could then attempt to isolate radio-induced effects from the raw bus signals, potentially allowing continuous or passive reception without disrupting normal operation.

8.3. Future Work

In this work, we showed that subtle RF sensitivities of standard embedded devices can be exploited to realize covert radio receivers, e.g., to infiltrate data into air-gapped systems. Our initial exploration of the mechanism opens up several promising directions for future work.

Transmitted Waveforms and Modulation Schemes. In our experiments, we validated receiver sensitivity using single-carrier RF signals and demonstrated successful reception of OOK-modulated data. Further work is needed to assess the feasibility of using more complex waveforms, such as pulsed ultra-wideband (UWB), frequency or phase-modulated, and multi-carrier signals.

Other Platforms. In our study, we focused on reception using STM32 MCUs, a microcontroller family found across a broad spectrum of commercial devices. Porting the mechanism to other MCU families is left for future work. Further, FPGAs constitute an interesting target for sensitivity assessment, given their large configuration space. We also believe that the approach could extend to other platforms such as smartphones and laptops. However, further work is required to assess whether data exposed at the operating-system level offers sufficient fidelity for reliable signal reception.

Bidirectional Communication. We leave the demonstration of bidirectional wireless communication between two airgap devices for future work. From a physical standpoint, such a setup is clearly viable – for instance, prior work like NoiseSDR [4] demonstrates how signal transmission can be realized using standard embedded devices. Integrating such a transmitter with our reception mechanism poses no conceptual barrier, requiring additional system integration and tuning.

9. Related Work

In this section, we give an overview of relevant literature on IEMI applications in a security context and airgap research. Moreover, we summarize prior works on turning embedded devices into radio receivers and elaborate how our work differs from these proposals.

IEMI and Sensor Security. Most research on IEMI has focused on malicious remote manipulation of sensors, showing that a wide range of modalities can be affected, including temperature sensors [61], accelerometers and gyroscopes [48], cameras [30], [35], [53], voltage and current sensors [67], capacitive touchscreens [62], speed sensors [59], barometric pressure sensors [40], [41], analog sensors in biomedical implants [38], and infrared sensors [57].

A related line of research investigates IEMI to tamper with device-internal communication buses [29], [69]. Adversaries have also leveraged infrastructure and peripherals, using fluorescent lamps [66], wired headphones [32], or grounding paths [31] to aid IEMI-based sensor manipulation. While not related to IEMI, prior research has demonstrated that sensors can be exploited for covert data transfer, e.g., using microphones, light, and magnetic sensors on smartphones to transfer digital data [27], [60].

Bridging the Airgap. As discussed in the Introduction, airgap infiltration has received relatively little attention, with prior work by Guri et al. [20], [24], [26], Kuhnnapfel et al. [37], and Kasmi et al. [33].

Exfiltration of data from air-gapped system has first been studied by Kuhn and Anderson [36]. Their “Soft TEMPEST” approach used a display to control the amplitude of emitted electromagnetic (EM) signals from software. Since then, many subsequent works, e.g., [1], [5], [19], [22], [23], [24], [25], [58], [68], have studied various hardware components and leakage sources. In the context of electromagnetic leakage, Camurati et al. [4] presented Noise-SDR, allowing use complex modulation schemes on device-internal leakage sources. In contrast, SpiralSpy [43] and DiskSpy [64] are passive approaches that rely on cooling fans and hard disk vibrations, respectively, to modulate externally applied radar signals.

Embedded Devices as Radio Receivers and Differentiation from Previous Work. Kasmi et al. [33] and Esteves [14], [44] first explored the use of IEMI for covert communication, employing kilowatt-range radio transmissions to manipulate temperature sensor readings at data rates of roughly 2.5 bit/s. To the best of our knowledge, this remains the only work to leverage IEMI effects to bridge the airgap. In contrast, our reception mechanism does not rely on the availability of sensors and furthermore exhibits sensitivity for low-power RF signals as small 1 mW.

Several projects have demonstrated creative ways of realizing software-defined radios (SDRs) by augmenting embedded platforms with external RF front-end circuitry such as antennas, filters, and amplifiers. Examples include ARM Radio on STM32 MCUs [12], [16], PiccoloSDR [3] and PicoSDR [13] on the Raspberry Pi Pico, and FPGA-based receivers [9], [47]. These works showcase the flexibility of embedded hardware, but share common requirements: external components (at least antennas, often amplifiers or filters), high-speed sampling and digital signal processing, and high resource usage to realize radio reception. Our approach is fundamentally different: we show that completely unmodified, sensor-less embedded devices can act as covert radio receivers with no external hardware and minimal signal processing requirements for realistic attack scenarios on low-resource embedded platforms.

10. Conclusion

In this paper, we studied parasitic RF sensitivities in conventional embedded systems. We introduced a structured methodology for their discovery and conducted a

comprehensive evaluation, revealing that such sensitivities occur in all 14 tested devices. These vulnerabilities allow adversaries with code execution on the target device – without any dedicated radio hardware – to receive wireless communication signals over significant distances, enabling command-and-control links into air-gapped systems, even under non-line-of-sight conditions. Our findings challenge fundamental assumptions about the physical isolation of electronic devices and call for a reassessment of security models that rely on such isolation.

Acknowledgements

This work was in part funded by the Deutsche Forschungsgemeinschaft (DFG, German Research Foundation) under Germany's Excellence Strategy - EXC 2092 CaSa - 390781972.

LLM usage considerations

LLMs were used for editorial purposes in this manuscript, and all outputs were inspected by the authors to ensure accuracy and originality.

Ethics considerations

All experiments were conducted on devices purchased by the authors and exclusively in shielded environments. No human subjects or sensitive personal data were involved, and the experiments did not interfere with other systems. Our findings do not directly compromise product security or pose immediate risk to vendors or users, as the evaluated devices employ mechanisms that prevent unauthorized firmware modification. The study examines the RF reception sensitivities of device hardware. While these properties could be relevant in scenarios involving firmware modification, no real-world attacks or circumventions of device protections were performed. As stated in the paper, we notified the respective manufacturers to enable them to assess potential implications.

References

- [1] I. Agadakos, C.-Y. Chen, M. Campanelli, P. Anantharaman, M. Hasan, B. Copos, T. Lepoint, M. Locasto, G. F. Ciocarlie, and U. Lindqvist, "Jumping the Air Gap: Modeling Cyber-Physical Attack Paths in the Internet-of-Things," in *Proceedings of the 2017 Workshop on Cyber-Physical Systems Security and PrivaCy*, Dallas Texas USA: ACM, Nov. 2017, pp. 37–48. [Online]. Available: <https://dl.acm.org/doi/10.1145/3140241.3140252>
- [2] B. R. Archambeault and J. Drewniak, *PCB design for real-world EMI control*. Springer Science & Business Media, 2013, vol. 696.
- [3] J.-L. Aufranc, "PiccoloSDR – A Raspberry Pi Pico powered SDR working with GNU Radio," 2021, accessed: November 13, 2025. [Online]. Available: <https://www.cnx-software.com/2021/03/11/picosdr-a-raspberry-pi-pico-powered-sdr-based-on-gnu-radio/>
- [4] G. Camurati and A. Francillon, "Noise-SDR: Arbitrary Modulation of Electromagnetic Noise from Unprivileged Software and Its Impact on Emission Security," in *2022 IEEE Symposium on Security and Privacy (SP)*. IEEE, 2022, pp. 1193–1210. [Online]. Available: <https://ieeexplore.ieee.org/document/9833767>
- [5] B. Carrara and C. Adams, "On Acoustic Covert Channels Between Air-Gapped Systems," in *Foundations and Practice of Security*, F. Cuppens, J. Garcia-Alfaro, N. Zincir Heywood, and P. W. L. Fong, Eds. Cham: Springer International Publishing, 2015, vol. 8930, pp. 3–16. [Online]. Available: https://link.springer.com/10.1007/978-3-319-17040-4_1
- [6] Code of Federal Regulation, "Part 15 - radio frequency devices," 2025, accessed: November 13, 2025. [Online]. Available: <https://www.ecfr.gov/current/title-47/chapter-1/subchapter-A/part-15>
- [7] N. Communications and I. Agency, "NIA – NATO Information Assurance," 2025, accessed: November 13, 2025. [Online]. Available: <https://www.ia.nato.int/niapc/tempest/certification-scheme>
- [8] A. Cui and R. Housley, "BADFET: Defeating Modern Secure Boot Using Second-Order Pulsed Electromagnetic Fault Injection," in *11th USENIX Workshop on Offensive Technologies (WOOT 17)*. Vancouver, BC: USENIX Association, Aug. 2017. [Online]. Available: <https://www.usenix.org/conference/woot17/workshop-program/presentation/cui>
- [9] dawsonjon, "Digital AM radio reception using digital LVDS inputs as 1-bit adcs," accessed: November 13, 2025. [Online]. Available: <https://github.com/dawsonjon/FPGA-radio>
- [10] G. Y. Dayanikli, "Electromagnetic interference attacks on cyber-physical systems: Theory, demonstration, and defense," Ph.D. dissertation, Virginia Tech, 2021.
- [11] A. Dehbaoui, J.-M. Dutertre, B. Robisson, and A. Tria, "Electromagnetic Transient Faults Injection on a Hardware and a Software Implementations of AES," in *2012 Workshop on Fault Diagnosis and Tolerance in Cryptography*. Leuven, Belgium: IEEE, Sep. 2012, pp. 7–15. [Online]. Available: <https://ieeexplore.ieee.org/document/6305224/>
- [12] A. Di Bene, "ARM radio: a project for the ARM MCU design contest," 2025, accessed: November 13, 2025. [Online]. Available: <https://www.i2phd.org/armradio/index.html>
- [13] J. Dvořák, "Pico SDR," 2025, accessed: November 13, 2025. [Online]. Available: <https://blog.porucha.net/2024/pico-sdr/>
- [14] J. L. Esteves, "Electromagnetic interference and information security: characterization, exploitation and forensic analysis," Ph.D. dissertation, HESAM Université, 2023. [Online]. Available: <https://theses.hal.science/tel-04155509v2>
- [15] European Commission, "Electromagnetic Compatibility (EMC) Directive," 2014, accessed: November 13, 2025. [Online]. Available: https://single-market-economy.ec.europa.eu/sectors/electrical-and-electronic-engineering-industries-eei/electromagnetic-compatibility-emc-directive_en
- [16] A. Garlassi, "ARM radio for system workbench," 2020, accessed: November 14, 2025. [Online]. Available: <https://hackaday.io/project/171053-arm-radio-for-system-workbench>
- [17] I. Gil and R. Fernández-García, "Characterization and modelling of EMI susceptibility in integrated circuits at high frequency," in *International Symposium on Electromagnetic Compatibility – EMC Europe*. IEEE, 2012, pp. 1–6. [Online]. Available: <https://ieeexplore.ieee.org/document/6396869>
- [18] A. Goldsmith, *Wireless Communications*. USA: Cambridge University Press, 2005.
- [19] M. Guri, "Air-Gap Electromagnetic Covert Channel," *IEEE Transactions on Dependable and Secure Computing*, vol. 21, no. 4, pp. 2127–2144, Jul. 2024. [Online]. Available: <https://ieeexplore.ieee.org/document/10197447/>
- [20] M. Guri and D. Bykhovsky, "aIR-Jumper: Covert air-gap exfiltration/infiltration via security cameras & infrared (IR)," *Computers & Security*, vol. 82, pp. 15–29, May 2019. [Online]. Available: <https://www.sciencedirect.com/science/article/pii/S0167404818307193>
- [21] M. Guri and Y. Elovici, "Bridgeware: the air-gap malware," *Communications of the ACM*, vol. 61, no. 4, pp. 74–82, Mar. 2018. [Online]. Available: <https://dl.acm.org/doi/10.1145/3177230>

[22] M. Guri, A. Kachlon, O. Hasson, G. Kedma, Y. Mirsky, and Y. Elovici, "GSMem: Data Exfiltration from Air-Gapped Computers over GSM Frequencies," in *24th USENIX Security Symposium (USENIX Security 15)*, 2015, pp. 849–864. [Online]. Available: <https://www.usenix.org/conference/usenixsecurity15/technical-sessions/presentation/guri>

[23] M. Guri, G. Kedma, A. Kachlon, and Y. Elovici, "AirHopper: Bridging the air-gap between isolated networks and mobile phones using radio frequencies," in *2014 9th International Conference on Malicious and Unwanted Software: The Americas (MALWARE)*. IEEE, 2014, pp. 58–67. [Online]. Available: <https://ieeexplore.ieee.org/abstract/document/6999418/>

[24] M. Guri, M. Monitz, Y. Mirski, and Y. Elovici, "BitWhisper: Covert Signaling Channel between Air-Gapped Computers Using Thermal Manipulations," in *2015 IEEE 28th Computer Security Foundations Symposium*, Jul. 2015, pp. 276–289. [Online]. Available: <https://ieeexplore.ieee.org/document/7243739>

[25] M. Guri, Y. Solewicz, A. Daidakulov, and Y. Elovici, "Fansmitter: Acoustic data exfiltration from (speakerless) air-gapped computers," *arXiv preprint arXiv:1606.05915*, 2016.

[26] M. Guri, Y. Solewicz, and Y. Elovici, "MOSQUITO: Covert Ultrasonic Transmissions Between Two Air-Gapped Computers Using Speaker-to-Speaker Communication," in *2018 IEEE Conference on Dependable and Secure Computing (DSC)*. Kaohsiung, Taiwan: IEEE, Dec. 2018. [Online]. Available: <https://ieeexplore.ieee.org/document/8625124/>

[27] R. Hasan, N. Saxena, T. Haleviz, S. Zawoad, and D. Rinehart, "Sensing-enabled channels for hard-to-detect command and control of mobile devices," in *Proceedings of the 8th ACM SIGSAC Symposium on Information, Computer and Communications Security*, ser. ASIA CCS '13. New York, NY, USA: Association for Computing Machinery, May 2013, pp. 469–480. [Online]. Available: <https://dl.acm.org/doi/10.1145/2484313.2484373>

[28] IEEE EMC Society, "Standards – EMC Society," 2025, accessed: November 13, 2025. [Online]. Available: <https://www.emcs.org/standards/>

[29] J. Jang, M. Cho, J. Kim, D. Kim, and Y. Kim, "Paralyzing Drones via EMI Signal Injection on Sensory Communication Channels," in *Proceedings 2023 Network and Distributed System Security Symposium*. San Diego, CA, USA: Internet Society, 2023. [Online]. Available: https://www.ndss-symposium.org/wp-content/uploads/2023/02/ndss2023_f616_paper.pdf

[30] Q. Jiang, X. Ji, C. Yan, Z. Xie, H. Lou, and W. Xu, "GlitchHiker: Uncovering vulnerabilities of image signal transmission with IEMI," in *32nd USENIX Security Symposium, USENIX Security 2023, Anaheim, CA, USA, August 9-11, 2023*, J. A. Calandrino and C. Troncoso, Eds. USENIX Association, 2023, pp. 7249–7266. [Online]. Available: <https://www.usenix.org/conference/usenixsecurity23/presentation/jiang-qinhong>

[31] Y. Jiang, X. Ji, Y. Jiang, K. Wang, C. Xu, and W. Xu, "PowerRadio: Manipulate Sensor Measurement via Power GND Radiation," in *Proceedings 2025 Network and Distributed System Security Symposium*. San Diego, CA, USA: Internet Society, 2025. [Online]. Available: <https://www.ndss-symposium.org/wp-content/uploads/2025-295-paper.pdf>

[32] C. Kasmi and J. Lopes Esteves, "IEMI Threats for Information Security: Remote Command Injection on Modern Smartphones," *IEEE Transactions on Electromagnetic Compatibility*, vol. 57, no. 6, pp. 1752–1755, Dec. 2015. [Online]. Available: <https://ieeexplore.ieee.org/document/7194754/>

[33] C. Kasmi, J. Lopes Esteves, and P. Valembois, "Air-gap Limitations and Bypass Techniques: "Command and Control" using Smart Electromagnetic Interferences," *The Journal on Cybercrime and Digital Investigations*, vol. 1, no. 1, pp. 13–19, Jan. 2016. [Online]. Available: <https://cyberjournal.cecif.fr/index.php/cybin/article/view/4>

[34] M. Kaur, S. Kakar, and D. Mandal, "Electromagnetic interference," in *2011 3rd International Conference on Electronic Computer Technology*, vol. 4. IEEE, 2011, pp. 1–5. [Online]. Available: <https://ieeexplore.ieee.org/document/5941844>

[35] S. Köhler, R. Baker, and I. Martinovic, "Signal Injection Attacks against CCD Image Sensors," in *Proceedings of the 2022 ACM on Asia Conference on Computer and Communications Security*. Nagasaki Japan: ACM, May 2022, pp. 294–308. [Online]. Available: <https://dl.acm.org/doi/10.1145/3488932.3497771>

[36] M. G. Kuhn and R. J. Anderson, "Soft tempest: Hidden data transmission using electromagnetic emanations," Springer, Tech. Rep., 1998.

[37] N. Kühnapfel, S. Preußler, M. Noppel, T. Schneider, K. Rieck, and C. Wressnegger, "LaserShark: Establishing Fast, Bidirectional Communication into Air-Gapped Systems," in *Proceedings of the 37th Annual Computer Security Applications Conference*, ser. ACSAC '21. New York, NY, USA: Association for Computing Machinery, Dec. 2021, pp. 796–811. [Online]. Available: <https://dl.acm.org/doi/10.1145/3485832.3485911>

[38] D. F. Kune, J. Backes, S. S. Clark, D. Kramer, M. Reynolds, K. Fu, Yongdae Kim, and Wenyuan Xu, "Ghost Talk: Mitigating EMI Signal Injection Attacks against Analog Sensors," in *2013 IEEE Symposium on Security and Privacy*. Berkeley, CA: IEEE, May 2013, pp. 145–159. [Online]. Available: <http://ieeexplore.ieee.org/document/6547107/>

[39] D. Kushner, "The real story of stuxnet," *IEEE Spectrum*, vol. 50, no. 3, pp. 48–53, Mar. 2013. [Online]. Available: <http://ieeexplore.ieee.org/document/6471059/>

[40] L. C. Lavau, M. Suhreke, and P. Knott, "Susceptibility of Sensors to IEMI Attacks," in *2021 IEEE International Joint EMC/SI/PI and EMC Europe Symposium*, Jul. 2021, pp. 533–537. [Online]. Available: <https://ieeexplore.ieee.org/document/9559197>

[41] —, "Impact of IEMI pulses on a barometric sensor," in *2022 International Symposium on Electromagnetic Compatibility – EMC Europe*, Sep. 2022, pp. 290–294. [Online]. Available: <https://ieeexplore.ieee.org/document/9900930>

[42] —, "Securing Temperature Measurements: An Assessment of Sensors' Vulnerability to IEMI," in *2023 International Symposium on Electromagnetic Compatibility – EMC Europe*, Sep. 2023, pp. 1–6. [Online]. Available: <https://ieeexplore.ieee.org/document/10274337>

[43] Z. Li, B. Chen, X. Chen, H. Li, C. Xu, F. Lin, C. X. Lu, K. Ren, and W. Xu, "SpiralSpy: Exploring a Stealthy and Practical Covert Channel to Attack Air-gapped Computing Devices via mmWave Sensing," in *Proc. NDSS*, 2022, pp. 1–16. [Online]. Available: https://www.research.ed.ac.uk/files/284657742/SpiralSpy_LI_DOA04112021_VOR.pdf

[44] J. Lopes Esteves, "An Introduction to Intentional Electromagnetic Interference Exploitation," in *Embedded Cryptography 3*. John Wiley & Sons, Ltd, 2025, pp. 257–278. [Online]. Available: <https://doi.org/10.1002/9781394351930.ch13>

[45] P. Mathur and S. Raman, "Electromagnetic Interference (EMI): Measurement and Reduction Techniques." *Journal of Electronic Materials*, vol. 49, no. 5, 2020. [Online]. Available: <https://doi.org/10.1007/s11664-020-07979-1>

[46] A. Z. Mohammed, L. Jenkins, R. Hatch, G. Y. Dayanikli, C. Simpson, R. Gerdes, and H. Wang, "The IEMI Effect: On the Efficacy of PCB-Level Countermeasures in Adversarial Environments," in *2024 IEEE 9th European Symposium on Security and Privacy (EuroS&P)*. Vienna, Austria: IEEE, Jul. 2024, pp. 361–380. [Online]. Available: <https://ieeexplore.ieee.org/document/10628528/>

[47] B. Newhouse, "A bluetooth low energy radio using FPGA SERDES." [Online]. Available: <https://github.com/newhouseb/onebitb>

[48] A. Pahl, K.-U. Rathjen, and S. Dickmann, "Intended electromagnetic interference with motion detectors," in *2021 IEEE international joint EMC/SI/PI and EMC europe symposium*. IEEE, 2021, pp. 324–328. [Online]. Available: <https://ieeexplore.ieee.org/document/9559187>

[49] J. G. Proakis and M. Salehi, *Digital Communications*, 5th ed. Boston, Mass.: McGraw-Hill, 2008, literaturverz. S. 1109 - 1141.

[50] E. Puschner, T. Moos, S. Becker, C. Kison, A. Moradi, and C. Paar, "Red Team vs. Blue Team: A Real-World Hardware Trojan Detection Case Study Across Four Modern CMOS Technology Generations," in *2023 IEEE Symposium on Security and Privacy (SP)*. San Francisco, CA, USA: IEEE, May 2023, pp. 56-74. [Online]. Available: <https://ieeexplore.ieee.org/document/10179341/>

[51] M. Ramdani, E. Sicard, A. Boyer, S. B. Dhia, J. J. Whalen, T. H. Hubing, M. Coenen, and O. Wada, "The electromagnetic compatibility of integrated circuits – past, present, and future," *IEEE Transactions on Electromagnetic Compatibility*, vol. 51, no. 1, pp. 78–100, 2009.

[52] R. Redl, "Power electronics and electromagnetic compatibility," in *PESC Record. 27th Annual IEEE Power Electronics Specialists Conference*, vol. 1. IEEE, 1996, pp. 15–21.

[53] Y. Ren, Q. Jiang, C. Yan, X. Ji, and W. Xu, "GhostShot: Manipulating the Image of CCD Cameras with Electromagnetic Interference," in *Proceedings 2025 Network and Distributed System Security Symposium*. San Diego, CA, USA: Internet Society, 2025. [Online]. Available: <https://www.ndss-symposium.org/wp-content/uploads/2025-2065-paper.pdf>

[54] A. Richelli, "EMI susceptibility issue in analog front-end for sensor applications," *Journal of Sensors*, vol. 2016, 2016.

[55] J. Robertson and M. Riley, "The Big Hack: How China Used a Tiny Chip to Infiltrate U.S. Companies," *bloomberg.com*, Oct. 2018, accessed: November 13, 2025. [Online]. Available: <https://www.bloomberg.com/news/features/2018-10-04/the-big-hack-how-china-used-a-tiny-chip-to-infiltrate-america-s-top-companies>

[56] T. Roth, D. Nedospasov, and J. Datko, "wallet.fail: Hacking the most popular cryptocurrency hardware wallets," Talk presented at the 35th Chaos Communication Congress (35C3), 2018, accessed: November 13, 2025. [Online]. Available: https://media.ccc.de/v/35c3-9563-wallet_fail

[57] J. Selvaraj, G. Y. Dayanikli, N. P. Gaunkar, D. Ware, R. M. Gerdes, and M. Mina, "Electromagnetic induction attacks against embedded systems," in *Proceedings of the 2018 on Asia Conference on Computer and Communications*, 2018, pp. 499–510. [Online]. Available: <https://dl.acm.org/doi/abs/10.1145/3196494.3196556>

[58] C. Shen, T. Liu, J. Huang, and R. Tan, "When LoRa meets EMR: Electromagnetic covert channels can be super resilient," in *2021 IEEE Symposium on Security and Privacy (SP)*. IEEE, 2021, pp. 1304–1317. [Online]. Available: <https://ieeexplore.ieee.org/document/9519447>

[59] Y. Shoukry, P. Martin, P. Tabuada, and M. Srivastava, "Non-invasive spoofing attacks for anti-lock braking systems," in *Cryptographic Hardware and Embedded Systems - CHES 2013: 15th International Workshop, Santa Barbara, CA, USA, August 20-23, 2013. Proceedings 15*. Springer, 2013, pp. 55–72. [Online]. Available: https://link.springer.com/chapter/10.1007/978-3-642-40349-1_4

[60] V. Subramanian, S. Uluagac, H. Cam, and R. Beyah, "Examining the characteristics and implications of sensor side channels," in *2013 IEEE International Conference on Communications (ICC)*, Jun. 2013, pp. 2205–2210. [Online]. Available: <https://ieeexplore.ieee.org/document/6654855>

[61] Y. Tu, S. Rampazzi, B. Hao, A. Rodriguez, K. Fu, and X. Hei, "Trick or heat? Manipulating critical temperature-based control systems using rectification attacks," in *Proceedings of the 2019 ACM SIGSAC Conference on Computer and Communications Security*, 2019, pp. 2301–2315.

[62] K. Wang, R. Mitev, C. Yan, X. Ji, A.-R. Sadeghi, and W. Xu, "GhostTouch : Targeted attacks on touchscreens without physical touch," in *31st USENIX Security Symposium (USENIX Security 22)*, 2022, pp. 1543–1559. [Online]. Available: <https://www.usenix.org/conference/usenixsecurity22/presentation/wang-kai>

[63] L. Wouters, "Glitched on earth by humans: A black-box security evaluation of the spacex starlink user terminal," Talk presented at Black Hat USA 2022, 2022, accessed: November 13, 2025. [Online]. Available: <https://i.blackhat.com/USA-22-Wednesday/US-22-Wouters-Glitched-On-Earth.pdf>

[64] W. Xu, D. Wen, J. Liu, Z. Lin, Y. Zheng, X. Xu, and J. Han, "DiskSpy: Exploring a Long-Range Covert-Channel Attack via mmWave Sensing of μ m-level HDD Vibrations," in *Proceedings of the 34th USENIX Conference on Security Symposium*. USA: USENIX Association, 2025. [Online]. Available: <https://www.usenix.org/conference/usenixsecurity25/presentation/xu-weiyi>

[65] C. Yan, W. Xu, and J. Liu, "Can you trust autonomous vehicles: Contactless attacks against sensors of self-driving vehicle," *Def Con*, vol. 24, no. 8, p. 109, 2016.

[66] F. Yang, W. Cui, X. Li, C. Yan, X. Ji, and W. Xu, "LightAntenna: Characterizing the Limits of Fluorescent Lamp-Induced Electromagnetic Interference," in *Proceedings 2025 Network and Distributed System Security Symposium*. San Diego, CA, USA: Internet Society, 2025. [Online]. Available: <https://www.ndss-symposium.org/wp-content/uploads/2025-2334-paper.pdf>

[67] F. Yang, Z. Dan, K. Pan, C. Yan, X. Ji, and W. Xu, "ReThink: Reveal the Threat of Electromagnetic Interference on Power Inverters," in *Proceedings 2025 Network and Distributed System Security Symposium*. San Diego, CA, USA: Internet Society, 2025. [Online]. Available: <https://www.ndss-symposium.org/wp-content/uploads/2025-691-paper.pdf>

[68] Z. Zhan, Z. Zhang, and X. Koutsoukos, "BitJabber: The World's Fastest Electromagnetic Covert Channel," in *2020 IEEE International Symposium on Hardware Oriented Security and Trust (HOST)*. San Jose, CA, USA: IEEE, Dec. 2020, pp. 35–45. [Online]. Available: <https://ieeexplore.ieee.org/document/9300268/>

[69] Y. Zhang and K. Rasmussen, "Electromagnetic Signal Injection Attacks on Differential Signaling," in *Proceedings of the 2023 ACM Asia Conference on Computer and Communications Security*, ser. ASIA CCS '23. New York, NY, USA: Association for Computing Machinery, Jul. 2023, pp. 314–325. [Online]. Available: <https://dl.acm.org/doi/10.1145/3579856.3590326>

Appendix A. Effect of ADC oversampling

We now examine how the ADC oversampling ratio affects the device's RF reception sensitivity. Oversampling increases the number of acquired samples per signal period, which can improve the effective resolution SNR of the received signal. As shown in Figure 21, the sensitive frequency regions remain largely unchanged across all oversampling ratios (left), indicating that oversampling does not shift the inherent spectral response of the device. However, the SNR in dB improves almost linearly with every doubling of the oversampling ratio (right) until reaching a plateau at an oversampling factor of approximately 32.

These findings show that oversampling, like expected, can substantially enhance the received signal quality, potentially allowing the attacker to trade transmission rates against more reliable data reception.

Appendix B. Device Orientations

We placed the device in the xz , xy , and yz planes and rotated it by 0° and 90° . The resulting frequency responses

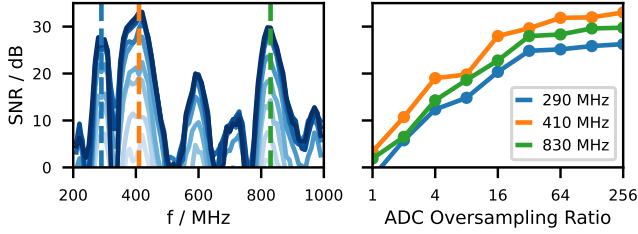


Figure 21: Effect of the ADC oversampling ratio on reception sensitivity SNR.

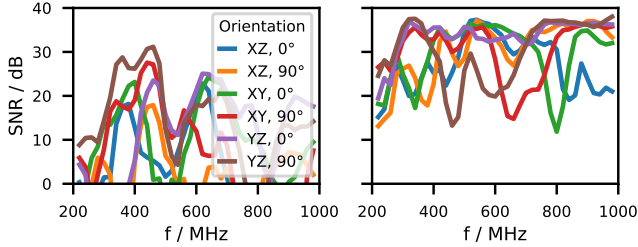


Figure 22: SNR over frequency for two reception paths with the device oriented in the xz , xy , and yz planes, each rotated by 0° and 90° .

are shown in Figure 22. While the detailed spectral characteristics vary across orientations, the sensitivities remain significant and correlated in frequency, indicating that orientation affects but does not eliminate the phenomenon.

Appendix C. Recommended Path Configurations

See the recommended path configurations in Table 3.

TABLE 3: Recommend path configurations.

PUPD	Output Value	Mode	Output Type	Output Speed (Not Relevant)	
1	Pull-Down	High	Input	Open-Drain	Medium
2	Pull-Down	High	Output	Open-Drain	Medium
3	Pull-Down	High	Alternate Function	Open-Drain	Medium
4	Pull-Down	High	Analog	Open-Drain	Medium
5	Pull-Up	Low	Input	Open-Drain	Medium
6	Pull-Up	Low	Output	Open-Drain	Medium
7	Pull-Up	Low	Alternate Function	Open-Drain	Medium
8	Pull-Up	Low	Analog	Open-Drain	Medium